VALIDATION OF COMPUTATIONAL FLUID DYNAMICS CODE MODELS FOR USED FUEL DRY STORAGE SYSTEMS

I1. Gregory Banken[1], I2. Kamran Tavassoli[2], I3. Jayant Bondre[3]

[1]President, Q-Metrics, Inc., [2]Manager of Thermal Analysis, Transnuclear, Inc., [3]V.P. of Engineering, Transnuclear, Inc.

Abstract

Computational fluid dynamics (CFD) codes have been used to validate the system designs for used nuclear fuel storage and transportation applications. The reliance on and the importance to safety of these codes has grown with the drive to increase the capacity of these systems. The higher capacities of today's designs have increased the total decay heat dissipation from each package from below 10 kW in the 1990's to over 40 kW today. Higher decay heats require more thermally efficient designs to maintain system component and fuel cladding temperatures below their design limits. This results in the need to increase the accuracy of the analytical methods in addition to improving the thermal efficiency of the system.

While CFD codes have provided a powerful tool for analyzing the thermal performance of complex designs, the validity of the results provided by the codes are only as good as the numerical models and choices in evaluation options used. In particular, the means used to determine the convective heat transfer coefficients and radiation exchange are critical to accurately predicting the temperature distribution within the storage or transportation system. In the current study, we explore the analytical steps necessary to achieve validation of the FLUENT CFD code models against the test results for one of Transnuclear's used fuel dry storage systems and the CFD code model's subsequent implementation in the analysis of another higher capacity system. The required steps include the choice of meshing scheme, fixed versus temperature dependant thermal properties, choice of turbulence modeling approach and wall function, and the use of steady-state versus transient modeling techniques to capture the turbulent nature of the heat transfer regime.

1.0 INTRODUCTION

The Advanced NUHOMS® System is one of the used fuel dry storage systems designed by Transnuclear, Inc., which provides for the horizontal, dry storage of canisterized Spent/Used Fuel Assemblies (SFA) at the Independent Spent Fuel Storage Installation (ISFSI). The Advanced NUHOMS® System includes:

- A Dry Shielded Canister (DSC) that provides confinement, an inert environment, structural support, and criticality control for PWR fuel assemblies, and
- A reinforced concrete storage overpack designated as the Advanced Horizontal Storage Module (AHSM) that provides for the passive removal of the spent fuel's decay heat, environmental and seismic protection for the DSC, and radiological shielding from the DSC's contents.

The AHSM is designed to passively remove decay heat from the DSC via a combination of radiation, conduction and convection. The bulk of the decay heat is rejected from the DSC to the AHSM air space by convection and then removed from the AHSM by the buoyancy driven circulation of air flow through the AHSM. Ambient air enters the AHSM through a ventilation inlet opening located in the lower front wall of the AHSM, circulates around the DSC and the heat shield, and then exits through an outlet opening located in the top of the AHSM. Heat is also radiated from the DSC surface to the heat shield and AHSM walls where it is transferred to the AHSM air space via convection and conducted through the walls. For the thermal protection of the AHSM concrete, a thin heat shield is installed on the inside of the base storage unit. The passive cooling system for the AHSM is designed to assure that SFA peak cladding temperatures and concrete temperatures during long term storage remain below acceptable limits to ensure fuel cladding integrity. The air flow paths through AHSM are illustrated in Figure 1.

The safety basis of storing a DSC within the AHSM was established in the UFSAR [7] by using FLUENT™ code [5]. While other analysis techniques had been previously used to predict the thermal-hydraulic

environment within the AHSM, the application of computational fluid dynamics (CFD) allowed the evaluation of the flow distribution and the convection heat transfer rates to be based on first principles and not assumptions and semi-empirical correlations. The FLUENT™ code chosen for this evaluation is a general purpose CFD code that offers the following modeling capabilities as they relate to this application:

- Meshing flexibility using structured and unstructured mesh generation with hexahedra, non-hexahedra, and tetrahedral mesh types
- Capability to model low speed, buoyancy driven flow regimes
- Steady-state and transient flows
- Inviscid, laminar, and turbulent flows
- Heat transfer including forced, natural, and mixed convection, conjugate heat transfer, and radiation
- Custom materials property database
- Choice of a variety of turbulence modeling techniques

A key to gaining the acceptance of the CFD modeling results as the safety basis for the licensing of the Advanced NUHOMS® system was the validation of the FLUENT™ code for computing the buoyancy driven flow within the enclosure of the NUHOMS®-7P system with mixed convection, conjugate heat transfer, and radiation. The NUHOMS®-7P system is similar in heat transfer mechanism to the Advanced NUHOMS® System. In the NUHOMS®-7P system, a DSC is also stored horizontally inside a concrete overpack with inlet air vents at the bottom, outlet air vents at the top, and heat shields protecting the concrete walls. The validation of the FLUENT™ CFD code for handling the convection and radiation heat transfer included the modeling of the full scale test results for a NUHOMS®-7P system [6]. It is the steps required and the lessons learned from this validation process that is the focus of this paper.

2.0 VALIDATION OF FLUENT™ COMPUTER CODE

The applicability of the FLUENT™ software code for predicting the thermal-hydraulic performance of a Horizontal Storage Module (HSM) was validated using the full scale test results for the NUHOMS®-7P HSM. This performance testing [6] was conducted using a combination of electrical heaters and actual spent fuel assemblies to establish the thermal performance of both the HSM and the NUHOMS®-7P DSC housed within it. While the design and decay heat loading of the NUHOMS®-7P HSM varies from a typical AHSM, the general arrangement and thermo-physical principles driving the airflow through the modules are similar for both designs.

Figure 2 illustrates the layout of the NUHOMS®-7P HSM array as tested. As seen, the test setup consisted of three (3) HSMs arranged side-by-side. The figure also illustrates the placement of the two (2) inlet vents and two (2) outlet vents per HSM. A comparison of the layout of the HSM in Figure 2 with the layout of the AHSM in Figure 1 demonstrates the similarity between the flow paths for the two designs. As shown in Figure 2, the air distribution chamber of the NUHOMS®-7P HSM is equipped with three openings, one in the front baffle and two on each side of the chamber roof to enhance the air distribution within the main vault.

Figure 3 illustrates the thermocouple locations used in the testing [6] and, by extension, the locations at which a direct comparison between measured and predicted temperatures are possible. The numbers in the figures represent the thermocouple identification number per the legend provided in each figure. Only the center HSM and one side HSM were instrumented for the test. The combined measurement uncertainty for the thermocouples, the extension wires, and the data acquisition system was estimated at $\pm$4ºC (7ºF). While this level of combined measurement uncertainty is in-line with the typical measurement error of $\pm$1% of the absolute temperature, it also represents an important consideration that should be included in the comparison of measured to predicted results.

The material properties used for this analysis were taken from ASME 1992 [4] for carbon and stainless steel components, Rohsenow (1998) [3] for air, and Fintel (1974) [2] for the concrete. The soil below the basemat of the HSM is assumed to have a constant earth temperature of 70°F. While the use of temperature dependant properties for the solid components can improve modeling accuracy, the set of properties with the most direct impact are those for air since even a slight change with temperature affects the calculation of both the convective heat transfer rates and the level of the buoyancy forces that drive the airflow rate.

The CFD modeling of the NUHOMS®-7P DSC in the HSM was based on the geometry shown in Figure 2. Figure 4 provides an isometric wire frame view of the thermal-hydraulic model developed for this evaluation. As seen, the CFD model represents a three dimensional simulation of the center HSM of the array depicted in Figure 2.

As shown in Figure 4, the model accurately captures the geometry of the twin inlet vents. The dimensions and offset turns of the modeled duct match the actual flow path within the HSM. The model also includes an accurate representation of the forward air distribution plenum within its triple air ducts leading to the main vault within the HSM, the I-beam support structure, and the two exhaust air ducts leading to the roof of the HSM.

The modeling of the DSC within the HSM is accomplished using only shell elements since the heat transfer within the DSC's fuel basket was not simulated. The decay heat loading is simulated as a uniform heat flux applied over the length of the DSC shell between the shield plugs. The heat shields are modeled using thin conducting plate elements.

2.1 Modeling Considerations

Given the numerical intensity of a CFD calculation, a prudent step in its application is to examine the problem for potential modeling considerations that can be made without significantly impacting the results. For the modeling of the NUHOMS®-7P DSC in the HSM the following steps were considered to simplify the model and avoid excessive mesh density and run time.

a) The screened openings at the front of the HSM were simulated as simple inlet opening with an equivalent loss coefficient based on standard flow fittings [1] instead of creating a detailed model.
b) Similarly, the final flow turn within the outlet shielding blocks, the outlet opening, and the wire mesh at the screened exhaust openings are not specifically modeled. Instead, a combined set of flow loss factors for these items [1] is applied as a flow resistance element at the outlet.
c) Subtle shifts in the location and/or size of various components in the CFD model permitted the alignment of these components and avoided the creation of mesh elements with extremely small aspect ratios.
d) Divide the flow regime into zones of high and low mesh resolution needs in order to focus the computational resources on the areas of the model that require it.
e) The diurnal cycle in the solar heating of the exterior surfaces of the HSM was simplified from a set of time dependant values to an equivalent daily averaged heat loading.

The flow losses associated with flow paths that match standard flow fittings have been well defined by experimental testing [1]. The modeling of these flow paths can be greatly simplified by applying an equivalent flow loss factor. Since these flow loss factors can be defined as constant, quadratic, or exponential functions of the flow velocity, the non-linear nature of the loss factor can be accurately captured. The application of a loss factor for simplification steps a and b above was judged to have a minimum effect on the predicted thermal-hydraulic performance within the HSM cavity. Similarly, the location/size changes for alignment purposes as part of simplification step c are limited to a fraction of one percent of the total length and, therefore, judged to have an insignificant impact on the overall results.

The ability of the FLUENT™ program to create non-conformal computational meshes is used to increase the mesh density in those areas requiring greater fluid flow and/or thermal resolution and decrease the mesh density in those areas (i.e., within the concrete walls, etc.) that do not experience large thermal gradients. Figure 4 illustrates an elevation view of the mesh profile along the y-z plane through the center of the HSM. The non-conformal nature of the mesh is evident from the figure with the mesh density being significantly higher in the region of the inlet plenum, the DSC shell and shield plugs, and the outlet exhaust ducts and much lower elsewhere.

The variation in the solar heating on the exterior surfaces of the HSM with the time of the day would generally imply that a transient analysis was required. However, in this instance, the extended computational needs of a transient evaluation were avoided by the knowledge that the variation in solar heating principally affects only a relatively thin layer of the exterior concrete. In contrast, the temperatures of the DSC and the interior surfaces of the HSM are more closely aligned with the long term average level of the solar heating. As such, the transient evaluation was replaced with a steady-state evaluation by averaging the cumulative daily solar heating over 24 hours.

While a symmetry plane could have been assumed along a y-z plane through the center of the HSM, a full 3-D model was selected for this validation effort since the boundary conditions imposed by the test HSMs on either side of the modeled HSM were not the same.

2.2 Model Solution Control

The FLUENT™ code offers several options for controlling the solution. The analysis was conducted using a first order, upwind discretization solver scheme as an initial solution. This initial solution was then used as a re-start point for a refined solution using a second order discretization solver scheme.

The CFD analysis is conducted with radiation and turbulent flow enabled. The radiation view factors were calculated using a "surface-to-surface method" with an elevated number of rays per surface. The effects of flow turbulence are calculated using a "κ-ε" turbulence model with standard wall function, while the temperature-dependent fluid density is computed using the Boussinesq model.

2.3 Discussion of the Results

Figure 5 presents a summary of the surface temperature distributions predicted for the analyzed decay heat loading of 5,320 Watts within the DSC and the measured long term average ambient temperature of 77ºF. Table 1 presents a comparison of the test measured temperatures at the thermocouple locations and corresponding predicted temperatures at the same locations as obtained from the CFD model results. The CFD predicted results are rounded to the nearest whole degree since the exact location of the thermocouple is uncertain and since the model accuracy does not support reporting to the tenth of a degree.

A comparison of the measured vs. predicted temperatures at seven different locations on the exterior of the DSC shell (i.e., thermocouple IDs C-2-01 through C-2-13) provided in

Table 1 shows that the predicted shell temperatures consistently bound the measured temperatures. At the single location on the side of the DSC (i.e., thermocouple ID C-2-02), the predicted shell temperature is 17ºF higher than the test measurement, while the predicted temperatures along the bottom of the DSC are 30 to 65ºF higher than the test measurements (i.e., thermocouple ID C-2-03, C-2-11, and C-2-13). A review of the predicted flow pattern near the bottom of the DSC shows the expected region of low airflow between the DSC support rails which would raise the temperatures along the bottom of the DSC. One reason for the over-prediction of the temperatures on the bottom side of the DSC is that the predicted region of low airflow was not as severe or extensive as that predicted due to the support rail geometry differences that are not fully captured by the CFD model. In reality, the region of stagnate flow at the base of the DSC is probably not as complete as assumed by the modeling. Any increase in airflow in this region could significantly reduce the temperatures along the bottom of the DSC. The absence of modeling the heat transfer internal to the DSC also contributed to the noted temperature differences since, for the helium gas filled DSC, buoyancy forces will tend to shift the decay heat rejection away from the bottom of the DSC and towards the upper surfaces. This phenomenon is especially apparent for the NUHOMS®-7P fuel basket which uses a spacer disc type of design and where internal convection plays a significant role in the internal heat transfer.

A comparison of the predicted heat shield temperatures to the test measurements is provided in Table 1 at five (5) locations (i.e., thermocouple IDs HS-2-43 to HS-2-47). The predicted temperatures conservatively bound the measured temperatures, but within a relatively narrow margin of 4 to 14ºF.

The surface temperature of the HSM's concrete was measured at ten (10) locations (i.e., thermocouple IDs H-2-04 to H-2-25). A review of the predicted versus measured temperatures at these locations in Table 1 shows that the maximum measured concrete temperatures predictably occur on the underside of the roof slab (i.e., thermocouple IDs H-2-11, H-2-21, and H-2-25). The CFD model predicts an essentially constant temperature of 135 to 137ºF at these locations, while the measured temperatures indicates a slightly lower temperature at the center, inside surface of the roof slab (i.e., thermocouple ID H-2-11) than at either the front or the back. The predicted temperatures are within 3 to 6ºF of the measured temperatures at the front and back locations on the inside surface of the roof slab, but 11ºF hotter than the measured temperature at the center location.

The CFD model predicted sidewall temperature midway between HSMs conservatively bounds the measured temperature by 16ºF (i.e., thermocouple ID H-2-04), under estimates the inside surface temperature by 3ºF (i.e., thermocouple ID H-2-05), and over estimates the inside surface temperature at the intersection of the

sidewall and roof slabs (i.e., thermocouple ID H-2-10) by 22ºF. While the test report [6] is silent on this, it is suspected that the measured data at thermocouple ID H-2-10 is too low given the trend in the adjacent thermocouple locations.

The CFD model predicted roof exterior temperatures are within 4ºF at the center of the HSM (i.e., thermocouple ID H-2-17), bounds the measured temperature by 9ºF midway between adjacent HSMs (i.e., thermocouple ID H-2-16), and under predicts the measured temperature by 12ºF near the exhaust vents (i.e., thermocouple IDs H-2-19 and H-2-23). The bounding temperatures achieved in the center of the HSM would indicate that the methodology used for estimating the diurnal cycle in the solar loading on the roof surface was appropriate. The under estimate achieved for the concrete temperatures near the exhaust vents is probably related to the lack of modeling of the final turn in the exhaust flow under the shielding blocks. The model assumes that the exhaust air flows straight upwards into the ambient. In reality, the horizontal flow of the relatively hot exhaust air will provide some level of heating the concrete surface as it exits the screened opening.

The test [6] used six (6) thermocouples to monitor the exit air temperature from the two exhaust vents. These thermocouples (i.e., thermocouple IDs H-2-29, H-2-30, and H-2-31 for the rear exhaust vent and thermocouple IDs H-2-35, H-2-36, and H-2-37 for the front exhaust vent) indicate an average exhaust temperature of 119ºF for the rear vent and 116ºF for the front vent. In contrast, the CFD analysis indicates an average exhaust temperature of 140ºF for the rear vent and 136ºF for the front vent, or a temperature rise through the HSM that is approximately 50% higher than that indicated by the test exit air temperatures. Since a lower temperature rise equates to lower buoyancy forces and an associated lower airflow rate through the HSM, the predicted temperatures within the HSM would need to be much higher in order to support the exit air temperatures indicated by the test results. A more likely explanation is that, given the location of the thermocouples at the face of the screened outlet and the relatively low flow rate through the openings, a significant level of mixing with the ambient air probably occurred.

Figure 6 provides representative illustrations of the airflow profile within the HSM. The figures demonstrate that relatively even flow distribution is achieved over the length of the DSC. Areas of flow re-circulation are present in the forward and main air plenums beneath the DSC and between the support rails for the DSC.

In conclusion, the predicted absolute temperatures are within 10% of the absolute test measured temperatures with the exception of one test point (i.e., thermocouple C-2-13). The use of absolute temperatures for comparison is appropriate since radiation heat transfer plays a significant role in determining the temperature distribution within the HSM. The average error across all 28 thermocouple locations is less than 3%.

3.0 CONCLUSION AND LESSONS LEARNED

CFD modeling of the Advanced NUHOMS® System was critical to establishing the safety basis of the design for storing a DSC dissipating up to 24 kW of decay heat and obtaining a certificate of compliance from the NRC for this purpose. An important step in this process was the validation of the FLUENT™ software code for predicting the thermal-hydraulic performance of an Advanced NUHOMS® System by demonstrating its ability to produce representative thermal-hydraulic results for full-scale test of the NUHOMS®-7P HSM. This was successfully accomplished based on the results presented above. The lessons learned during this modeling and validation process included the following:

1) In order to reduce the size of the computational mesh for the CFD modeling, simplification steps can be considered to take advantage of existing and well established experimentally determined flow resistances through standard types of fittings and passages, such as inlet/outlet screens. Flow paths can also be lumped together as flow resistances to reduce the mesh density in non-critical paths.

2) Subtle design dimension changes to align various components of the modeled system are recommended to avoid the creation of mesh elements with extremely small aspect ratios. These changes will not affect the results significantly but can greatly improve the computational efficiency of the model.

3) The use of non-conformal computational meshes is recommended to allow an increase in the mesh density in areas where greater fluid flow and/or thermal resolution is required, while minimizing

the impact on the overall mesh count. This approach can also greatly increase the computational efficiency of the modeling and improve the accuracy of the results.

4) Radiation exchanges are critical to accurately predicting the temperature distribution within the typical nuclear storage or transportation system. Therefore, an accurate geometric representation of the system design and assignment of component emissivity are critical to accurately predicting the system temperatures. A robust radiation modeling technique that permits the independent assignment of emissivity and absorption properties to the various surfaces and refined resolution of the model surfaces is recommended for determining the radiation exchanges. For the FLUENT code, the discrete ordinates (DO) method is recommended. The DO method discretizes the radiative transport equations into a finite number of solid angles with the resolution of the control angle surface controlled by angular discretization and pixelation. Since the DO model is solved on the same finite volume mesh as the flow and convective heat transfer equations, a 1x1 pixelation and three angular divisions in the theta direction and three angular divisions along phi is usually sufficient for the typical mesh resolution used for modeling the flow regime.

5) The high decay heat dissipation associated with today's nuclear storage or transportation system will typically yield flow regimes in the turbulent region. The accurate determination of turbulent convection heat transfer coefficients is highly dependent on the near-wall mesh density and the choice of wall function. The calculation is further complicated by the fact that, under buoyancy driven flows, the near-wall velocities are typically higher than those remote from any surface. This is opposite of the situation under forced convection flows. As such, achieving appropriate 'y+' values for the mesh could require near-wall mesh densities that vary by location on the surface. The appropriate y+ value will depend on the near wall treatment chosen as part of the turbulence modeling. A y+ value of 30 to 90 is appropriate for standard wall functions, while a value between 1 and 3 is appropriate for enhanced wall functions.

REFERENCES

1 Idelchik, I. E., *Handbook of Hydraulic Resistance*, 3rd Edition, 1994.

2 Fintel, Mark, *Handbook of Concrete Engineering*, Van Nostraund Reinhold Company, September 1974.

3 Roshenow, W. M., J. P. Hartnett, and Y. I. Cho, *Handbook of Heat Transfer*, 3rd Edition, 1998.

4 American Society of Mechanical Engineers, *Boiler & Pressure Vessel Code*, Section III, 1992 Edition with Addenda through 1994.

5 FLUENT, Inc., *FLUENT™*, *Version 6.1*, Lebanon, NH, 2003.

6 Pacific Northwest Laboratory & Carolina Power and Light Company, *NUHOMS® Modular Spent-Fuel Storage System: Performance Testing*, Report PNL-7327/UC-812/EPRI NP-6941, September 1990.

7 Transnuclear, Inc., *Updated Final Safety Analysis Report for the Standardized Advanced NUHOMS® Horizontal Modular Storage System for Irradiated Nuclear Fuel*, ANUH-01.0150, Rev. 3, August 2008.

Table 1 Test vs. Predicted Temperatures for NUHOMS®-7P DSC in HSM

Thermocouple ID	Thermocouple Location Description	Test Temperature, ℉	FLUENT Predicted Temperature, ℉
C-2-01	Top of DSC, 9'-3" from front of HSM	239.9	250
C-2-02	Side of DSC, 9'-3" from front of HSM	197.4	214
C-2-03	Bottom of DSC, 9'-3" from front of HSM	162.5	192
C-2-10	Top of DSC, 5'-2" from front of HSM	212.5	231
C-2-11	Bottom of DSC, 5'-2" from front of HSM	145.8	182
C-2-12	Top of DSC, 15'-6" from front of HSM	203.7	245
C-2-13	Bottom of DSC, 15'-6" from front of HSM	133.0	198
H-2-04	Midway between adjacent HSMs, slightly above vertical centerline of DSC, 9'-3" from front of HSM	103.1	119
H-2-05	Inside wall of HSM, at vertical centerline of DSC, 9'-3" from front of HSM	121.5	119
H-2-10	Inside corner of HSM's vault, 9'-3" from front of HSM	101.7	124
H-2-11	Inside surface of HSM's roof, center of HSM, 9'-3" from front of HSM	124.5	136
H-2-16	Roof surface, midway between adjacent HSMs, 9'-3" from front of HSM	83.5	92
H-2-17	Outside surface of HSM's roof, center of HSM, 9'-3" from front of HSM	88.7	93
H-2-19	Outside surface of HSM's roof, center of HSM, 15'-6" from front of HSM	108.7	97
H-2-21	Inside surface of HSM's roof, center of HSM, 15'-6" from front of HSM	132.3	135
H-2-23	Outside surface of HSM's roof, center of HSM, 5'-2" from front of HSM	109.0	97
H-2-25	Inside surface of HSM's roof, center of HSM, 5'-2" from front of HSM	130.6	137
H-2-29	Right side of rear vent exit (looking aft), approximately 8" from side	117.9	134
H-2-30	Center of rear vent exit (looking aft)	120.9	141
H-2-31	Left side of rear vent exit (looking aft), approximately 8" from side	119.1	134
H-2-35	Right side of front vent exit (looking aft), approximately 8" from side	114.4	136
H-2-36	Center of front vent exit (looking aft)	120.4	146
H-2-37	Left side of front vent exit (looking aft), approximately 8" from side	113.9	137
HS-2-43	Horizontal heat shield, center of HSM, 5'-2" from front of HSM	143.4	157
HS-2-44	Vertical heat shield, approx. 8" up from bottom, 9'-3" from front of HSM	108.7	113
HS-2-45	Horizontal heat shield, center of HSM, 7'-2" from front of HSM	148.3	156
HS-2-46	Horizontal heat shield, center of HSM, 9'-3" from front of HSM	150.3	158
HS-2-47	Horizontal heat shield, center of HSM, 15'-6" from front of HSM	140.0	154

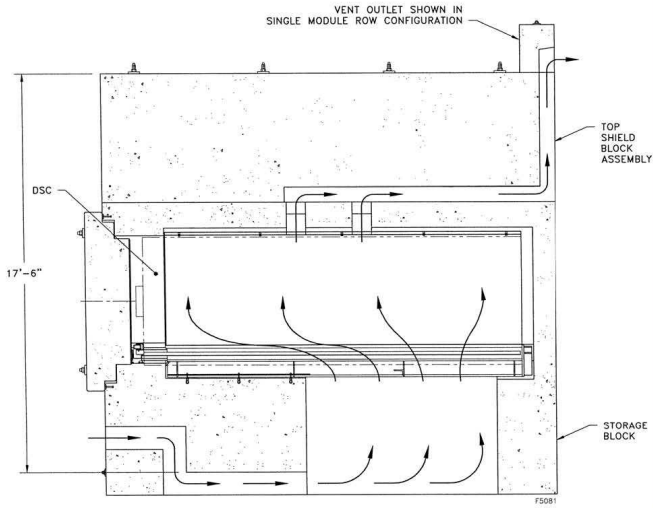

Figure 1 Illustration of Air Flow Paths through AHSM

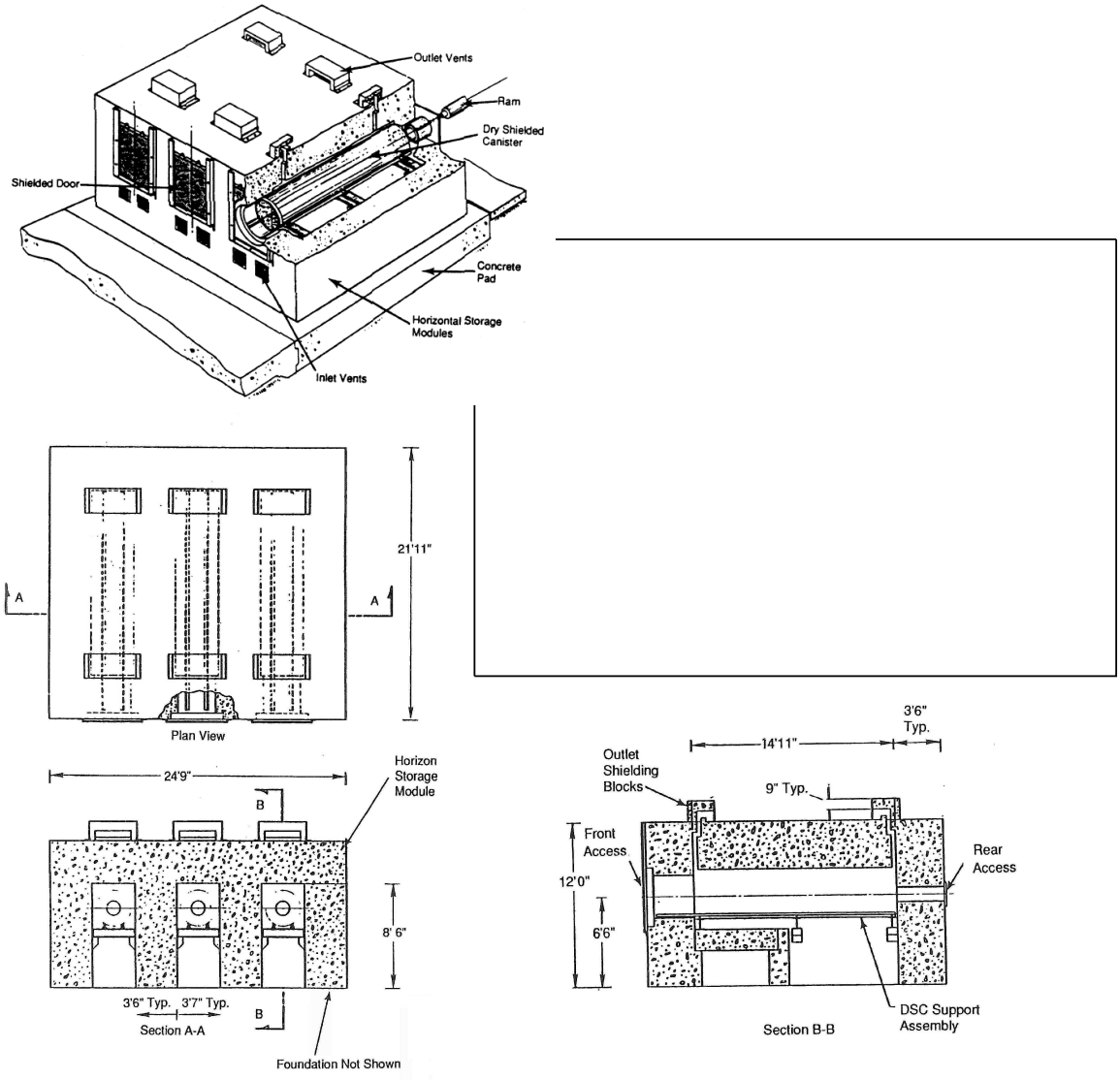

Figure 2 Layout of NUHOMS®-7P HSM Array for Performance Testing

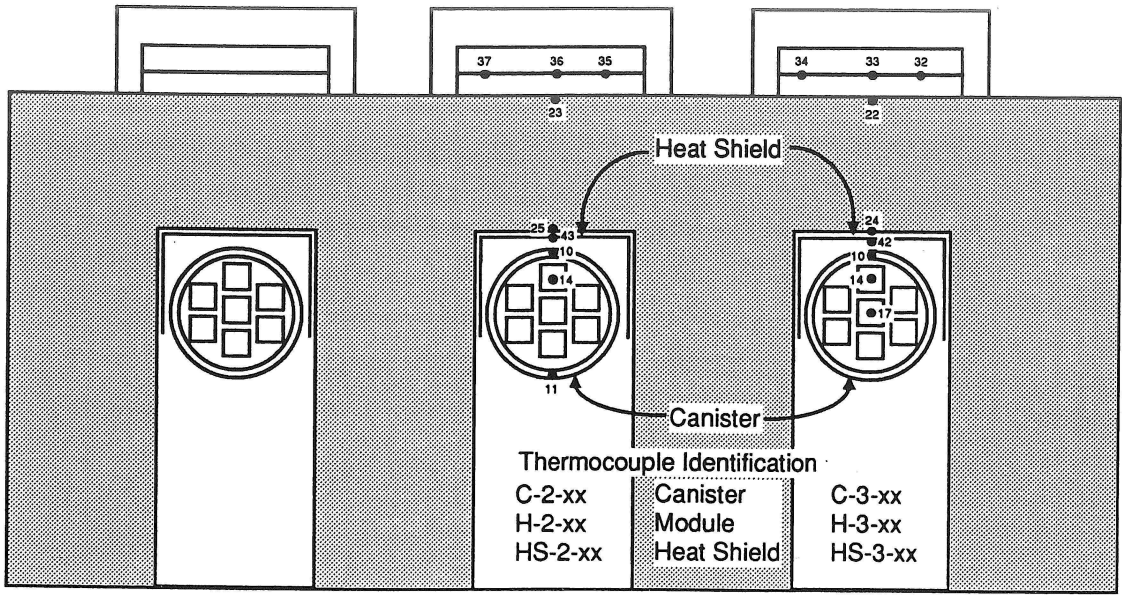

Thermocouple Locations 5′-2″ from Front of HSMs

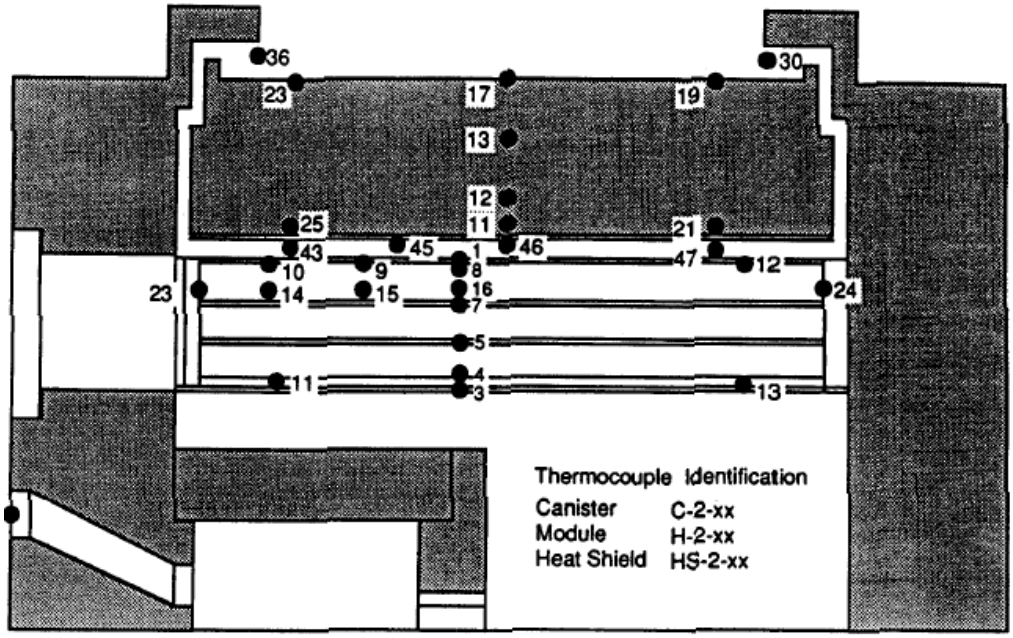

Center HSM (HSM-2)

Figure 3 Thermocouple Locations for Performance Testing

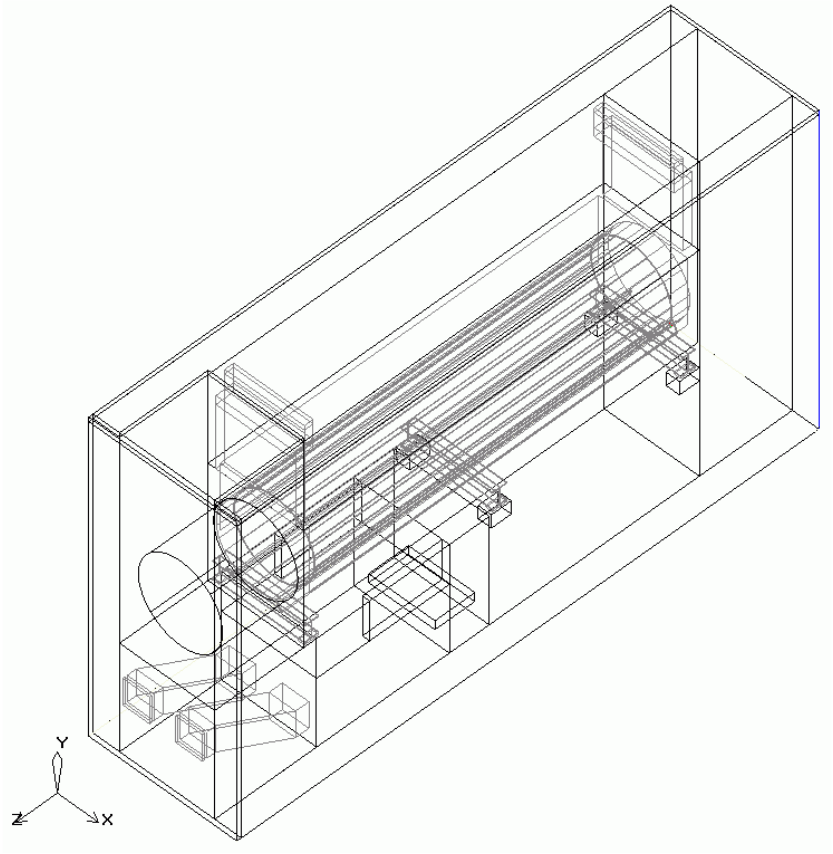

Isometric, Wireframe View

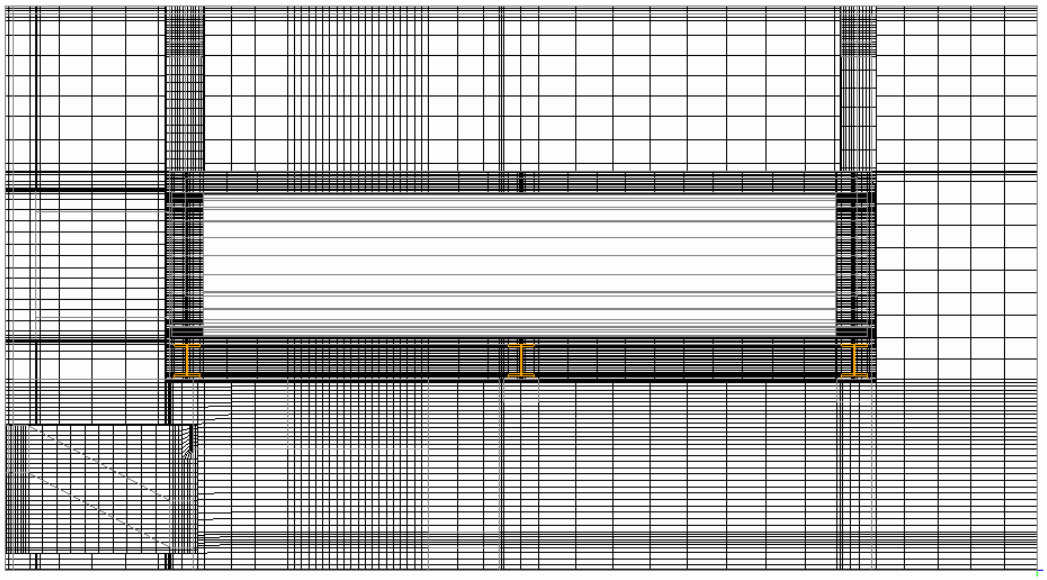

Elevation View of Meshing along Axial Center Plane of NUHOMS®-7P HSM

Figure 4 NUHOMS®-7P System FLUENT Model Layout

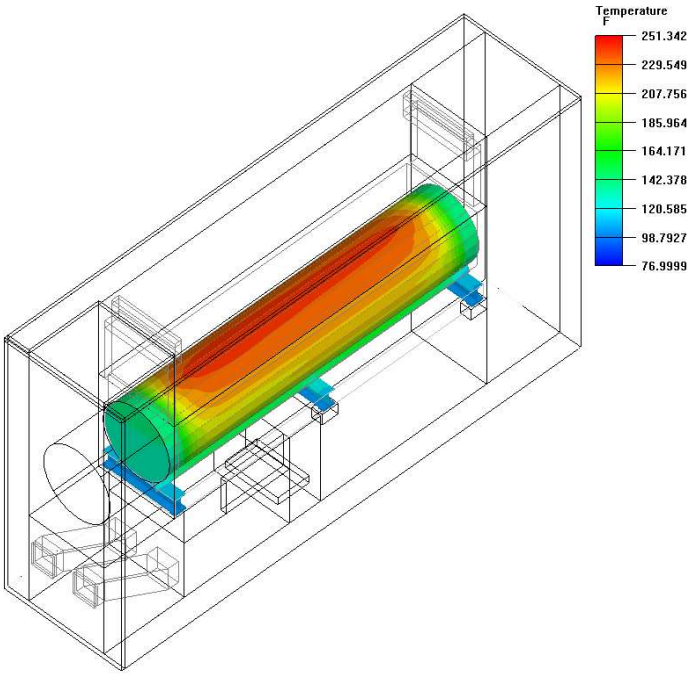

Temperature Distribution on NUHOMS®-7P DSC Surface

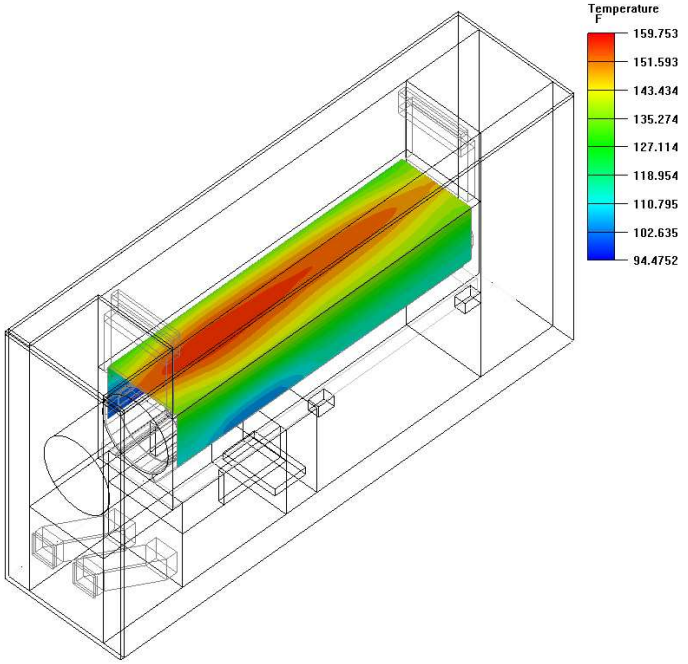

Temperature Distribution on Heat Shield Surfaces

Figure 5 Temperature Distributions on NUHOMS®-7P System FLUENT Model

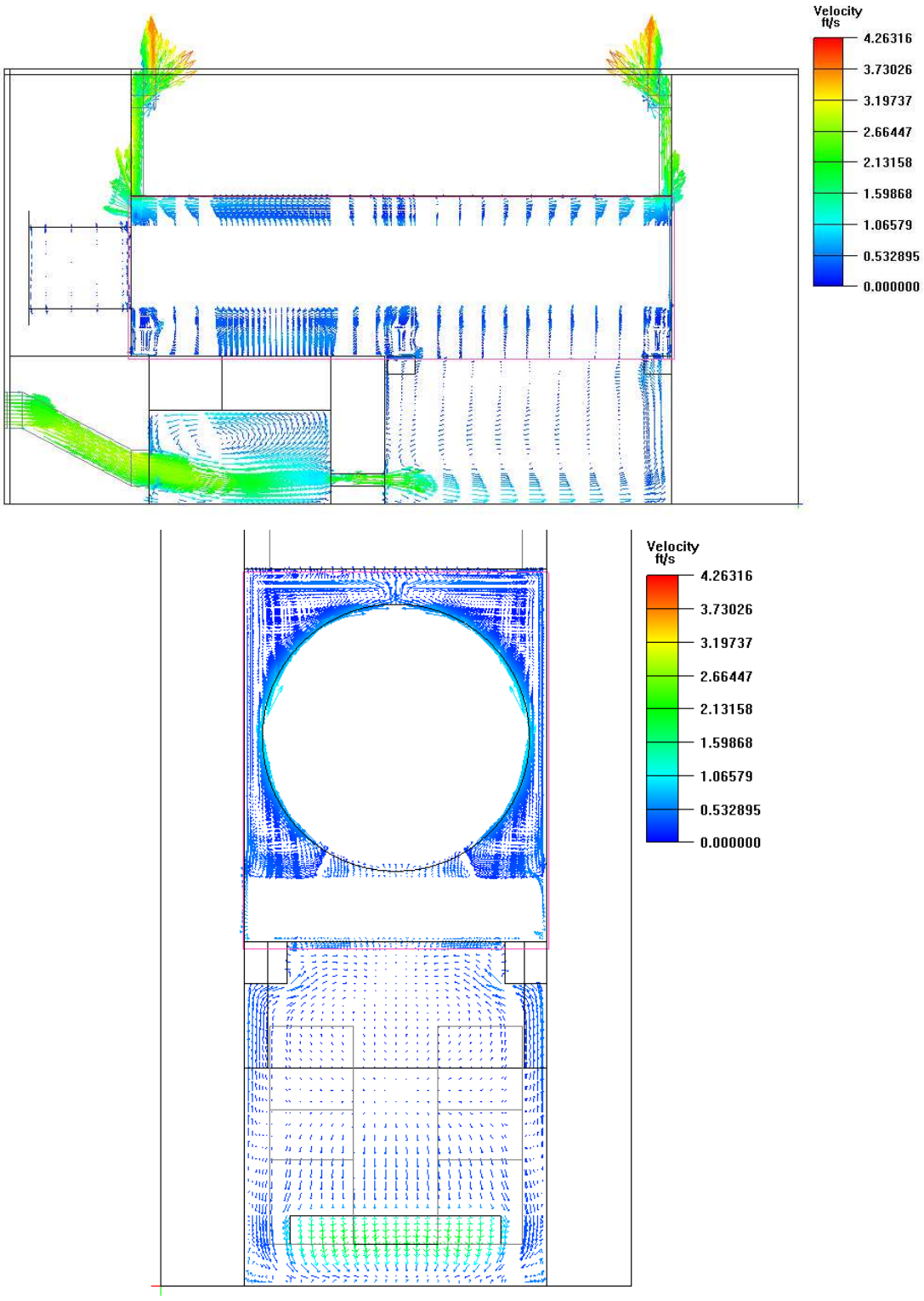

Figure 6 Velocity Profiles of the NUHOMS®-7P System FLUENT Model